Impact of annealing temperature on martensite transformations and structure of quaternary $Ti_{50}Ni_{47.7}Mo_{0.3}V_2$ alloy

Anatoliy Klopotov[1], Victor Gunther[1], Ekaterina Marchenko[1], Gulsharat Baigonakova[1], Timofey Chekalkin[2*], Ji-soon Kim[3], Ji-hoon Kang[3]

[1]*Research Institute of Medical Materials, Tomsk State University, ul. 19 Gv. Divizii 17, Tomsk, 634045, Russia*
[2]*Material Research Laboratory, Kang & Park Medical Co., 48 Jungsimsangeob-2 ro, Cheongju 28119, South Korea*
[3]*School of Material Science and Engineering, University of Ulsan, 93 Daehak-ro, Ulsan, 44610, South Korea*

[*]Corresponding author, Tel: +82-070-7702-8728; E-mail: tc77@mail2000.ru

Received: 09 August 2016, Revised: 05 October 2016 and Accepted: 22 November 2016

DOI: 10.5185/amlett.2017.7023
www.vbripress.com/aml

Abstract

Within the wide family of shape memory alloys (SMAs), TiNi-based alloys are characterized by unique characteristics, with good workability in the martensite phase and good resistance to corrosion and fatigue. In the nearest future, TiNi-based SMAs are expected the second birth to begin regarding their practical application, especially in creating a new material generation showing enhanced characteristics for clinical goals. Such a kind of expectations is naturally supposed to make a search among alloying elements for TiNi-based SMAs, as well as studies of adjacent effects in order to improve material properties. The objective of the work is to investigate the effect of heat treatment on the structure and properties of the quaternary $Ti_{50}Ni_{47.7}Mo_{0.3}V_2$ SMA, as potentially promising for medical devices. Specimens were prepared and annealed at 723, 923, 1123 K for 1 h. It was found that the studied alloy was in a multiphase state: TiNi-based intermetallic in three crystallographic modifications (austenite *B2*-phase and martensitic *R*- and *B*19′structures) and secondary $Ti_2Ni(V)$ phase. The increase of the annealing temperature doesn't affect the martensite transformation (MT) sequence $B2 \leftrightarrow R \leftrightarrow B19'$, but leads to a growth in lattice parameter of the parent phase. The most remarkable effect on the studied alloy was at 723 K. Volume fraction of $Ti_2Ni(V)$ precipitates in the structure was also maximum. It owes their presence to the shift of the MT points toward the lower temperature range. The temperature vs resistivity $\rho(T)$ curves show a characteristic shape, which is typical for TiNi-based SMAs with a two-step nature of the $B2 \leftrightarrow R \leftrightarrow B19'$ MT.

Keywords: TiNi-based alloy, martensite transformation, characteristic temperatures, heat treatment.

Introduction

TiNi-based SMAs showing shape memory effect (SME) are of great scientific and practical interest due to their unique physical and mechanical properties. [**1**, **2**]. They're more important for what they do than for what they are, since their use in medicine and bioengineering is also suggested by their good biocompatibility and the mechanical behavior, which is more similar to biological tissue response compared with other metallic materials applied for biomedical devices [**2**, **3**, **4**]. TiNi-based SMAs are basically functional materials. They have a complex of functional properties in combination with good mechanical properties [**5**]. Heat treatment has a significant effect on the structural and phase states, and leads to a change both the MT sequence and temperature ranges of MT [**6**].

Changing the alloy composition and performing mechanical treatment, it is possible to modify the characteristic parameters of SME, such as the maximum thermally recovering strain, the MT characteristic points, and the hysteresis properties. Ternary alloying of TiNi-based SMAs is ad rem undertaken with three major objectives as follows: (i) to improve the physico-mechanical characteristics of the overall alloy without making serious deviations in ductility and stiffness; (ii) to shift the MT characteristic points as far as they can be beneficial in applied problem, and (iii) to facilitate systematic understanding, from the structure exploring and evaluating, on the effect of additions by getting a clear insight and paradigm needed to further studies. No doubt, the alloying of TiNi-based SMAs with vanadium leads to changes in the physical and mechanical properties and to a change in the structural and phase states. Moreover, only limited research works on ternary TiNi(V)-based SMAs have been reported in published literature and no studies on quaternary TiNi(Mo,V)-based SMAs have been found [**7**, **8**, **9**].

Ternary alloying of TiNi-based SMAs by vanadium results to increase strength characteristics with keeping a

high level of plastic properties. Besides, the growth of strength when substituting V for Ni is due to an isolation of fine-dispersed phases from supersaturated solid solution, because of the local strain of the alloy atoms in the matrix provide resistance for dislocation movement. The ternary TiNiV SMAs, obtained by equal substitution of V for both Ti and Ni, have been already investigated focusing on their basic transformation behavior, SME, pseudoelasticity and wear characteristic as described in [**10**]. The temperatures of the one stage *B*2↔*B*19' MT drop down about 10 °C by adding 1–2 at.% V due to the effect of solid-solution strengthening. There appear many $(Ti,V)_2Ni$ precipitates within the matrix of both $Ti_{47.75}Ni_{49.25}V_3$ and $Ti_{47.25}Ni_{48.75}V_4$ alloys and oxygen atoms in the matrix were easily absorbed by the $(Ti,V)_2Ni$ second-phase particles to form the $(Ti,V)_4Ni_2O$ oxide.

Phase transformation behaviors, SME and mechanical properties of ternary TiNiMo-based SMAs, where Mo content is varied up to 2 at. %, are well known and investigated systematically, including porous SMAs [**1**, **11**, **12**, **13**]. There was found that the substitution of Mo for Ni in a $Ti_{51}Ni_{49}$ alloy induced the *B*2→*R* phase transformation, and the Mo addition within 1÷2 at.% will drastically lower the *Ms* down to -103 °C, while the *R* phase transformation points vary slightly. Thermo-mechanically treated $Ti_{51.0}Ni_{48.3}Mo_{0.7}$ SMA showed the two-stage MT even under the applied stress over 100 MPa, and the A_f almost did not change with the increasing applied stress, but kept constant at about 310 K, which is about the human body temperature. Furthermore, TiNiMo-based SMAs exhibit excellent mechanical properties and beneficial workability.

The production of semi-finished items of TiNi-based SMAs is supposed to undergo the material to multiple heat treatments. Therefore, it is necessary to know how the heat treatment will change the structure and physico-mechanical properties of the material in order to predict the behavior of a final implant. The objective of the present study is to explore the effect of heat treatment on the structural and physical properties of the cast $Ti_{50}Ni_{47.7}Mo_{0.3}V_2$ SMA. This paper aims also to provide a better understanding about the mechanism of MTs showed by the said alloy in evaluating the structural data.

Experimental

The quaternary $Ti_{50}Ni_{47.7}Mo_{0.3}V_2$ SMA for the study was fabricated by the vacuum induction melting (VIM) technology in a graphite crucible by remelting the Ti sponge and electrolytic Ni plates with addition of Mo and V. There were used melting and casting conditions optimized to prevent solidification cracks and reduce shrinkage pipe into the cast alloy, as described in [**14**]. Specimens were spark cut from as-received ingot by the electric-discharge wire-cut. All specimens for heat-treating were vacuum sealed in quartz tubes and then subjected to isothermal annealing in an electric furnace at temperatures of 723, 923 and 1123 K for 1 h followed by slow cooling in the furnace down to a room temperature.

To determine the behavior of MT, the electrical resistivity of the samples was measured by the four-point-probe method in temperature range from 240 to 370 K [**15**, **16**]. Ohmic contacts between the probes and samples were made using silver paste. The distance between the middle points along the length of the specimen was 10 mm and the potential difference when the MT occurs was measured by a digital multimeter and used for a plotting. A chromel-alumel thermocouple was attached upon the sample to measure the actual temperature. For tests below room temperature down to 240 K, liquid nitrogen was used as a coolant. Heating above room temperature was performed using an electrically heated air bath with adjustable power input. During this test the heating/cooling rate was 1 °C/min.

X-ray diffraction (XRD) analysis was carried out by DRON-4 and XRD-6000 (Shimadzu) diffractometer. Samples for microstructural studies were prepared according to standard procedures: they were ground, polished, and then etched in a solution of hydrofluoric and nitric acids. Details about the applied procedures can be found in [**17**, **18**]. Examinations of thin sections were carried out by OLYMPUS GX71 metallographic microscope with the DP70 digital camera.

Results and discussion

To determine the MT intervals in the $Ti_{50}Ni_{47,7}Mo_{0,3}V_2$ alloy, the $\rho(T)$ curves of nontreated alloy and after isothermal annealing at 723, 923 and 1123 K were drawn. Specific characteristics of such curves under cooling and heating have a typical appearance for TiNi-based SMAs with a two-step nature of the *B*2↔*R*↔ *B*19′ MT (where *B2* – cubic, *R* – rhombohedral, and *B*19′ – monoclinic lattice) (**Fig. 1**) [**1**, **6**].

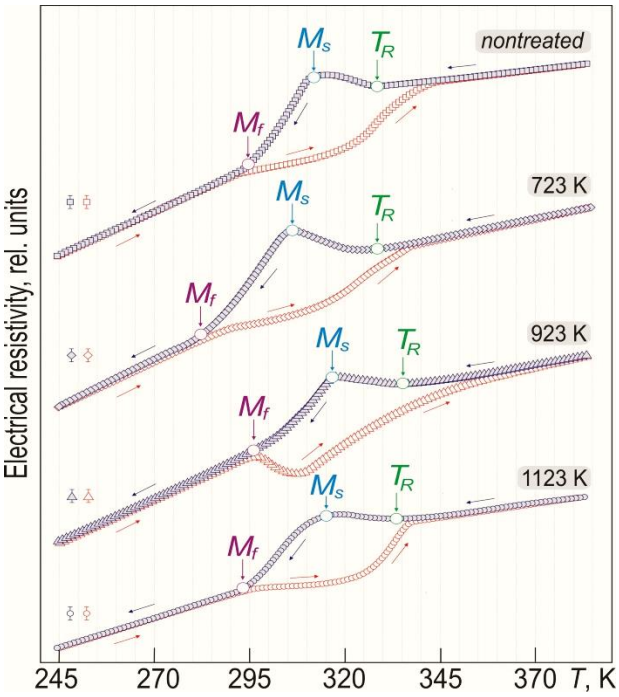

Fig. 1. Electrical resistivity vs temperature. Comparative curves of the $Ti_{50}Ni_{47.7}Mo_{0.3}V_2$ SMA after heat treatment, which comprise the MT characteristic points (T_R, M_s and M_f).

As seen, the isothermal annealing of the studied SMA at different temperatures leads to a change in the shape of

ρ(*T*) curves, and the MT hysteresis loop has no significant effect on the MT temperature range. The beginning of the deviation from the linearity on curves ρ(*T*) under cooling represents the start of the parent phase transition to the *R*-phase and corresponds to the T_R temperature of the *B*2→*R* MT. A sharp decrease in the resistivity under cooling on ρ(*T*) curves corresponds to the M_S point of direct *R*→*B*19′ MT. The M_f point shows the finish of the direct MT.

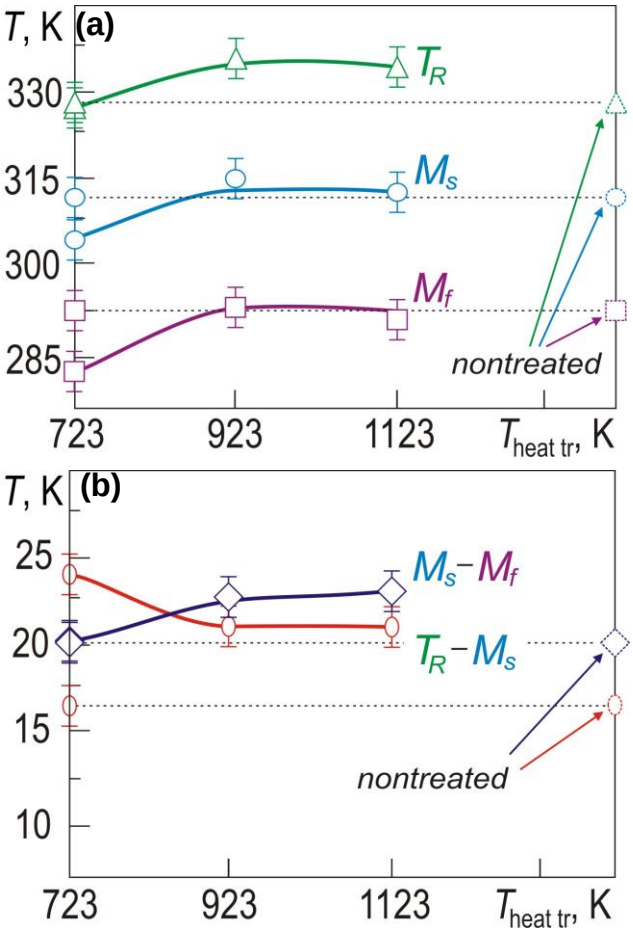

Fig. 2. MT characteristic points (*a*) – T_R, M_S, and M_f and residuals (*b*) – (M_S–M_f), and (T_R–M_S) vs temperature of annealing in the $Ti_{50}Ni_{47.7}Mo_{0.3}V_2$ SMA.

Based on the analysis of ρ(*T*) curves, characteristic points of the studied alloy were determined, and the effect of heat treatment was evaluated (**Fig. 2 (a)**). The data shown in **Fig. 2 (a)** demonstrate that the isothermal annealing at temperatures of 723, 923 and 1123 K has no significant effect on the characteristic temperatures. It can be seen that an increase in the temperature of annealing is accompanied with a slight increase in the T_R temperature in comparison with the initial state (**Fig. 1**). Characteristic points of the *R*→*B*19′ MT (T_R, M_S and M_f) in annealed alloys at temperatures of 923 and 1123 K are set as close to the initial ones. In addition, temperature ranges of *B*2→*R* and *R*→*B*19′ after annealing are slightly increased in comparison with the initial state (**Fig. 2 (b)**).

Such an increase in the MT temperature ranges, (T_R–M_S) and (M_S–M_f), on the temperature of annealing reflects in fact that there is a change in the structural and phase state that affects both the mobility of interphase boundaries during MTs and the MT driving force [**19**].

Thus, annealing of the $Ti_{50}Ni_{47.7}Mo_{0.3}V_2$ alloy leads to a noticeable change in the shape of resistivity curves in the MT range with a slight change in the characteristic MT temperatures. In order to characterize the contributions of *B*2→*R* and *R*→*B*19′ MT in the change of ρ(*T*) curves, the $(\Delta\rho_{B2\rightarrow R})/(\Delta\rho_{R\rightarrow B19'})$ ratio was determined in the studied alloy. $\Delta\rho_{B2\rightarrow R}$ characterizes the degree of deviation from linearity ρ(*T*) as a result of *B*2→*R* MT. It is defined as the difference between resistivity ρ_{Ms} at the M_S point for *R*→*B*19′ MT and resistivity ρ_{TR} at the T_R point for the *B*2→*R* MT (**Fig. 3 (a)**):

$$\Delta\rho_{B2\rightarrow R} = \rho_{Ms} - \rho_{TR} . \quad (1)$$

The presence of the second *R*→*B*19′ MT on the ρ(*T*) curve is observed as a sharp decrease in the resistivity near the M_S point (ρ_{Ms}) along. In this case, $\Delta\rho_{R\rightarrow B19'}$ characterizes the difference between resistivity ρ_{Ms} at the M_S point and resistivity ρ_{Mf} at the M_f point for the *R*→*B*19′ MT (see **Fig. 3 (a)**):

$$\Delta\rho_{R\rightarrow B19'} = \rho_{Ms} - \rho_{Mf} . \quad (2)$$

The dependence between ratio $(\Delta\rho_{B2\rightarrow R})/(\Delta\rho_{R\rightarrow B19'})$ and the temperature of annealing was drawn (**Fig. 3 (b)**).

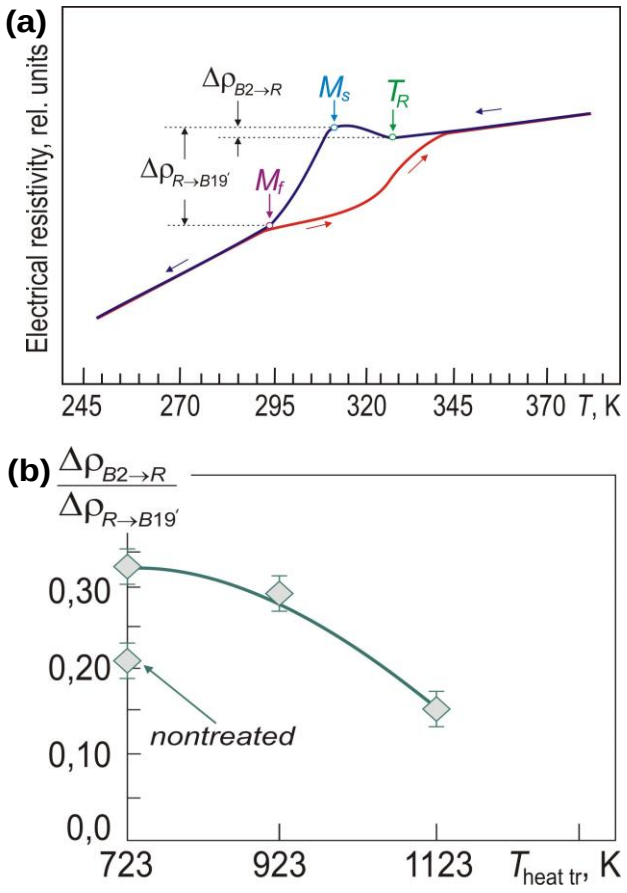

Fig. 3. Schematic representation of ρ(*T*) loop (*a*) (taking into consideration the contributions from *B*2→*R* and *R*→*B*19′ MTs) and ratio $(\Delta\rho_{B2\rightarrow R})/(\Delta\rho_{R\rightarrow B19'})$ vs temperature of annealing in the $Ti_{50}Ni_{47.7}Mo_{0.3}V_2$ SMA (*b*).

As seen, initially for the nontreated sample, the contribution from the B2→R MT, due to the deviation from the linear dependence within the TR-MS temperature range, is not high. The largest contribution to the ρ(*T*) dependence compared to the nontreated sample is observed after annealing at 723 K. A further increase in the annealing temperature leads to a remarkable decrease in the contribution of *B2→R* MT in the deviation from linear dependence of ρ(*T*). Annealing at a high temperature (over 1123 K) leads to a significant decrease in the contribution of *B2→R* MT compared to the nontreated sample.

It is to be noted the following important points that reflect the study of the annealing effect on $Ti_{50}Ni_{47.7}Mo_{0.3}V_2$ -based alloy, which was carried out by various methods. Based on the analysis of ρ(*T*), it has been shown that the annealing of the studied alloy does not affect significantly the characteristic temperatures of MT (**Fig. 1–2**). In addition, a significant change in the $(\Delta\rho_{B2\rightarrow R})/(\Delta\rho_{R\rightarrow B19'})$ has been revealed (**Fig. 3**).

The use of the XRD study also facilities to fix the effect of annealing on the structural change and phase state. **Fig. 4** shows the XRD pattern of the nontreated sample. XRD patterns were obtained at room temperature. According to the data of ρ(*T*) dependencies, the room temperature is about the end of the *R→B19′* MT (see **Fig. 1**).

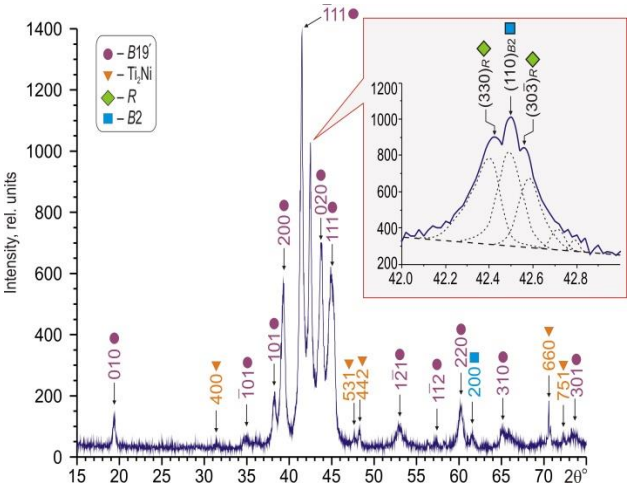

Fig. 4. XRD pattern of the nontreated $Ti_{50}Ni_{47.7}Mo_{0.3}V_2$ SMA, where: ● – *B*19′ martensite phase; ♦ – *R*-phase; ■ – *B*2 parent phase; ▼– Ti_2Ni precipitate.

Indexing XRD patterns makes it possible to establish that, at the room temperature, both the nontreated and annealed samples are in the multiphase state: TiNi(Mo,V)-based intermetallic in three crystallographic modifications (*B2, R* and *B*19′) and the secondary Ti_2Ni(V) phase. As seen, the parameter of the *B*2 unit cell in the treated alloys has a value which is higher than those in the nontreated sample (**Table 1**).

Based on XRD, geometric modeling of lines in the reflex within 42÷43° allows to distinguish three reflexes: $(110)_{B2}$, $(303)_R$, and $(30\bar{3})_R$ (**Fig. 5**). The evolution of the angular location and the intensity of reflexes both the *B*2 and the *R*-phase shows the change in the lattice parameter of these phases, as well as the ratio of intensities reflects the change in their volume fraction. Low intensity value of the reflexes compared to the ones of the *B*19′ martensitic phase shows a low volume fraction of these phases. This correlates with the data on ρ(*T*) test (see **Fig. 1**). The presence of reflexes from the parent phase indicates that the alloy is not fully transformed to the *R*-phase as a result of the *B2→R* MT.

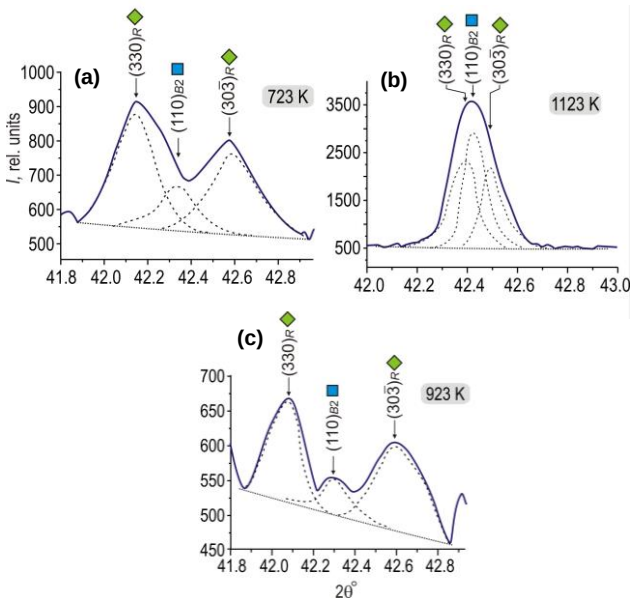

Fig. 5. XRD patterns of the $Ti_{50}Ni_{47.7}Mo_{0.3}V_2$ SMA treated at 723 (*a*), 923 (*b*) , and 1223 (*c*) K for 1 h, where: ♦ – *R*-phase; ■ – parent phase.

According to the value*s* of unit cell parameters for both *B*2- and *R*-phase, shown in **Table 1**, it can be seen that the maximum value of the rhombohedral distortion (*R*-phase distortion angle – α_R) is observed in the alloy after annealing at 923 K.

Table 1. Lattice parameters, grain size, and Ti_2Ni precipitate size in the treated $Ti_{50}Ni_{47.7}Mo_{0.3}V_2$ SMA .

$T_{heat\ tr}$, K	a_{B2}, nm	a_R, nm	α_R, °	Grain size, μm	Ti_2Ni size, μm
Nontreated	0.30086	0.90118	89.58	20±3	10±3
723	0.30188	0.90351	89.15	15±3	12±3
923	0.3029	0.90182	88.82	17±3	7±3
1123	0.3029	0.90106	89.51	12±3	5±3

In [**20**, **21**], using TiNi samples alloyed with third elements, it has been shown that α_R strictly depends on the alloying element, its content in TiNi composition, and the volume fraction of the *R*-phase.

As shown by the XRD, the alloy is not completely in the *R*-state, since about 3–5 % of *B*2 phase volume ratio keeps as long as the finish of the *(B2+R)→B19′* MT occurred. This also correlates with evaluation of ρ(*T*) curves (see **Fig. 1**). The observed increase in the unit cell parameters for both the *B*2 and the *R*-phase in the annealed samples is to underline an increase in Ti atoms having larger atomic size (R_{Ti}=0.1462 nm) compared to Ni atoms (R_{Ni}=0.1246 nm) in the parent phase.

By optical microscopy it was found that, in the $Ti_{50}Ni_{47,7}Mo_{0,3}V_2$ SMA after crystallization (nontreated), structures with areas of dendritic crystallization and coarse precipitates Ti_2Ni (10–15 μm), which have been randomly located within the grains, were off-eutectic formed. Besides, there were fine TiNiV precipitates separately crystallized in the matrix, and also $Ti_4Ni_2(V,O,N,C)$ precipitates round-shaped and segregated with a composition, confirmed as Ti-rich near equiatomic TiNi(V) phase. The average size of grains is 20±3 μm (**Fig. 6 (a)**; **Table 1**).

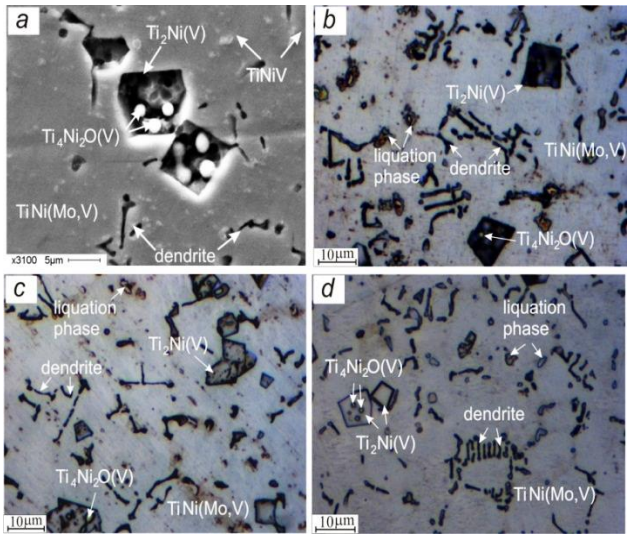

Fig. 6. Microstructure of the $Ti_{50}Ni_{47.7}Mo_{0.3}V_2$ SMA: nontreated (*a*) and after annealing at 723 (*b*), 923 (*c*), and 1123 K (*d*) for 1 h.

The microstructure of the studied alloy after annealing at 723 K for 1 h turned out to be changed (**Fig. 6 (b)**). Even intensive enrichment of grain bodies with $Ti_2Ni(V)$ compounds with an enlargement of 3-5 μm, where segregations of $Ti_4Ni_2O(V)$ precipitates are located, has occurred. The average grain size decreases in comparing to the nontreated alloy (see **Table 1**). The grain boundaries are substantially accurate, free from compounds and recover grains almost completely.

Increasing the annealing temperature up to 923 K is accompanied with suppression of the dendritic structure, and it becomes less branched. There is a decrease both in the overall volume fraction and the size of coarse $Ti_2Ni(V)$ precipitate down to 7±3 μm. The segregated phase grows little in grains, what increases the microstructural inhomogeneity of the alloy (**Fig. 6 (c)**; **Table 1**).

High annealing temperature (1123 K) leads to grain refinement down to 12±3 μm and formation of a poorly developed dendritic structure alongside grain boundaries. The average particle size of Ti_2Ni precipitate decreases compared to the nontreated alloy. Microstructural heterogeneity of the alloy also decreases due to the dissolution of most of segregated and $Ti_2Ni(V)$ precipitates in the matrix. The grain boundaries are partial and interrupted. The matrix becomes much clear (**Fig. 6 (d)**).

It well correlates with the data on XRD analysis and ρ(*T*) investigation as follows: the annealing results in a decrease in the microstructural inhomogeneity due to dissolution of most of the segregated phases and precipitates in the matrix. It is accompanied with a decrease in the volume fraction and the average particle size of the $Ti_2Ni(V)$-based precipitate and a more uniform redistribution of the eutectic inclusions alongside the grain boundaries. In Ti-rich SMAs, an increase in Ti concentration is known to have insignificant effect on the MT points [**1**, **22**, **23**]. This is also consistent with the data obtained from the ρ(*T*) study (**Fig. 1–2**). Based on the analysis of $(\Delta\rho_{B2\rightarrow R})/(\Delta\rho_{R\rightarrow B19'})$ ratio between the contribution from the *B*2→*R* MT and the *R*→*B*19′ MT, it can be suggested that a change in vanadium content in the matrix grains the structure, and an increase of Ti concentration as a result of annealing leads to such an evolution of the MT (**Table 2**). Despite the fact that annealing at 723, 923 and 1123 K for 1 h of the $Ti_{50}Ni_{47.7}Mo_{0.3}V_2$ SMA preserves a dendritic crystallization being inherent in the original alloy, it leads to a change in the distribution of structural components.

Table 2. Quantitative elemental data of the structural components in the nontreated $Ti_{50}Ni_{47.7}Mo_{0.3}V_2$ SMA

Component	Element, at. %				
	Ti	Ni	Mo	V	O
*B*2-matrix	47.66	50.06	0.15	2.27	–
$Ti_2Ni(V)$	63.43	35.88	–	0.69	–
TiNi(V)	36.43	33.25	–	30.32	–
$Ti_4Ni_2O(V)$	59.16	30.50	–	1.23	9.11

Conclusion

This study sheds considerable light on the potential of the impact of annealing temperature on the structural and physical properties of the cast $Ti_{50}Ni_{47.7}Mo_{0.3}V_2$ SMA. Experimental studies were conducted under varying the annealing temperature. The following conclusions can be drawn. The said SMA exhibits two-step MT *B*2↔*R*↔*B*19′ on both cooling and heating. The increase of annealing temperature leads to a growth of the lattice parameter of the *B*2 phase that is caused with dissolution of V in the matrix. The V addition (2 at. %) modifies the microstructure in such a way that fine-dispersed TiNiV, $Ti_2Ni(V)$, and $Ti_4Ni_2(V, O,N,C)$ precipitates are formed. In changing the annealing temperature we can effect on structural heterogeneity of the matrix, since the maximum Ti_2Ni precipitate size is revealed after annealing at 723 K because V reduces temperature of recrystallization of the Ti_2Ni phase. The growth of annealing temperature drastically changes the ρ(*T*) dependency. The studied alloy is most sensitive when the annealing temperature reaches 723 K. Isolation of $Ti_2Ni(V)$ particles at this heat treatment makes the characteristic points move toward the lower temperature area.

Acknowledgements

This study (research grant #8.1.42.2015) was supported by the Tomsk State University Academic D.I. Mendeleev Fund Program in 2015-2016.

Author's contributions

Conception/design of the study: AK,VG; Acquisition of data: EM, GB, JhK; Analysis and interpretation of data: AK, TC, JsK;

Wrote the manuscrip: TC; Manuscript editing/reviewing and conceptual advice: JsK. Authors have no competing financial interests. Authors give final approval of the version to be submitted and any revised version.

References

1. Gunther, V.E.; Hodorenko, V.N.; Chekalkin, T.L. et al. Medical materials and shape memory implants: In 14 vol. / Shape memory medical materials, Tomsk: MIC, **2011**, 1.
ISBN: 9785985890440
2. Muhamedov, M.; Kulbakin, D.; Gunther, V. et al.; *J. Surg. Oncol.*, **2015**, *111*, 231.
DOI: 10.1002/jso.23779
3. Kokorev, O.; Hodorenko, V.; Chekalkin, T. et al.; *Artif Cells Nanomed Biotechnol.*, **2016**, *44*, 704.
DOI: 10.3109/21691401.2014.982799
4. Petrini, L.; Migliavacca, F.; *J Metallurgy*, **2011**, ID 501483.
DOI: 10.1155/2011/501483
5. Gunther, V.E.; Chekalkin, T.L.; Kim , J.S. et al.; *Adv Mater Lett.*, **2015**, *6*, 8.
DOI: 10.5185/amlett.2015.5597
6. Gunther, V.E.; Dambaev, G.Ts.; Sysolyatin, P.G. et al. Delay law and new class of materials and implants in medicine, Northampton, MAA: STT, **2000**.
ISBN: 0970235305
7. Quin, M.P. U.S. Patent 4505767, **1985**.
8. Gyunter, V.; Baigonakova, G.; Marchenko, E.; Klopotov, A.; *Adv Mat Res.*, **201**5, *1085*, 299.
DOI: 10.4028/www.scientific.net/AMR.1085.299
9. Lin, H.; Lin, K.; Chang, S.; Lin, C.; *J Alloy Compd.*, **1999**, *284*, 213.
DOI: 10.1016/S0925-8388(98)00937-2
10. Lin, H.; Yang, C.; Lin, M. et al.; *J Alloy Compd.*, **2008**, *449*, 119.
DOI: 10.1016/j.jallcom.2006.01.136
11. Fushun, L.; Zhen, D.; Yan, L.; Huibin, X.; Phase. *Intermetallics*, **2005**, *13*, 357.
DOI: 10.1016/j.intermet.2004.07.024
12. Nam, T.; Chung, D.; Kim, J.; Kang, S.; *Mater Lett.*, **2002**, *52*, 234.
DOI: 10.1016/S0167-577X(01)00424-4
13. Jiang, H.; Rong, L.; *Mater Sci Forum*, **2007**, *546*, 2127.
DOI: 10.4028/www.scientific.net/MSF.546-549.2127
14. Raz, S.; Sadrnezhaad, S.; *Mater Sci Tech.*, **2004**, *20*, 593.
DOI: 10.1179/026708304225016680
15. Al-Aql, A.A.; Dughaish, Z.H.; Baig, M.R.; *Mater Lett.*, **1993**, *17*, 103.
DOI: 10.1016/0167-577X(93)90066-7
16. Khodorenko, V.N.; Gyunter, V.E.; Monogenov, A.N. et al.; *Tech. Phys. Lett.*, **2001**, *11*, 970.
DOI: 10.1134/1.1424409
17. *ASTM Standard F3122-14.*; ASTM International, West Conshohocken, **2014**.
DOI: 10.1520/F3122-14
18. Bramfitt, B.L.; Benscoter, A.O.; Metallographer's Guide: Practices and Procedures for Irons and Steel*;* ASTM International: Ohio, **2012**.
DOI: 10.1361/mgpp2002p169
19. Jani, J.M.; Leary, M.; Subic, A. et al.; *Mater. Design*, **2014**, *56*, 1078.
DOI: 10.1016/j.matdes.2013.11.084
20. Sun, X.; Ni, X.; Shen, J. et. al.; *J Alloy Compd.*, **2011**, *509*, 8323.
DOI: 10.1016/j.jallcom.2011.05.080
21. Singh, N.; Talapatra, A.; Junkaew, A. et al; *Comput Mater Sci*., **2016**, *112*, 347
DOI: 10.1016/j.commatsci.2015.10.029
22. Liu, X.; Wang, Y.; Yang, D.; Qi, M.; *Mater. Charact.*, **2008**, *59*, 402.
DOI: 10.1016/j.matchar.2007.02.007
23. Tadayyona, G.; Mazinania, M.; Guob, Y. et al.; *Mater. Charact.*, **2016**, *112*, 11.
DOI: 10.1016/j.matchar.2015.11.017